Drought cascades across multiple systems in Central Asia identified based on the dynamic space-time motion approach

Lu Tian[1], Markus Disse[1], Jingshui Huang[1]

[1]Chair of Hydrology and River Basin Management, Technical University of Munich, Arcisstrasse 21, 80333 Munich, Germany

Correspondence to: Lu Tian (lu.tian@tum.de)

Abstract. Drought is typically induced by the extreme water deficit stress that cascades through the atmosphere, hydrosphere, and biosphere. Cascading drought events could cause severe damage in multiple systems. However, identifying cascading drought connections considering the dynamic space-time progression remains challenging, which hinders further exploring the emergent patterns of drought cascades. This study proposes a novel framework for tracking drought cascades across multiple systems by utilizing dynamic space-time motion similarities. Our investigation focuses on the four primary drought types in Central Asia from 1980 to 2007, namely precipitation (PCP), evapotranspiration (ET), runoff, and root-zone soil moisture (SM), representing the four systems of atmosphere, hydrosphere, biosphere, and soil layer respectively. 503 cascading drought events are identified in this study, including the 261 four-system cascading drought events. Our results show a significant prevalence of the four-system cascading drought pattern in Central Asia with high systematic drought risk, mainly when seasonal PCP droughts with high severity/intensity and sizeable spatial extent are observed. As for the temporal order in the cascading drought events, ET droughts are likely to occur earlier than Runoff droughts after PCP droughts, and SM droughts are more likely to occur at last, implying the integrated driven effect of the energy-limited and water-limited phases on the drought progression in Central Asia. Our proposed framework could attain precise internal spatial trajectories within each cascading drought event and enable the capture of space-time cascading connections across diverse drought systems and associated hazards. The identification of cascading drought patterns could provide a systematic understanding of the drought evolution across multiple systems under exacerbated global warming.

1 Introduction

Droughts manifest as water deficits in the atmosphere (precipitation), hydrosphere (runoff), biosphere (evapotranspiration), and soil layer (soil moisture) (Orth and Destouni, 2018; Zargar et al., 2011), resulting in a sequential cascade of effects across interconnected atmospheric-hydrological-biological-agricultural systems. Anthropogenic global warming amplifies and accelerates this cascading drought chain impacting multiple system sections, exacerbating the underlying systematic risk (Gaupp et al., 2020; Yuan et al., 2023), and increasing uncertainty in predicting drought impacts (Cook et al., 2018; Lehner et al., 2017). Current research primarily focuses on the isolated consequences of precipitation deficits within certain sectors, such as agriculture security, water scarcity, and human health (Fouillet et al., 2006; Jones and van Vliet, 2018; Tuttle and Salvucci,

30   2017; Vicente-Serrano et al., 2013; Yusa et al., 2015). However, this compartmentalized approach fails to capture the interactions and spatial-temporal dependencies within the entire droughts network, which often results in an underestimation of risk as cascading natural hazards usually cause more severe impacts than any of the single hazard events alone. A comprehensive understanding of drought dynamics evolution across the water cycle necessitates an investigation into the spatiotemporal development of drought cascades. While some knowledge regarding the progression of drought from the

35   atmosphere (precipitation) to the hydrosphere (runoff), biosphere (evapotranspiration), and soil layer (soil moisture) exists at the catchment scale, this understanding remains limited when considering a larger scale. The complexities arise from interactions among multiple systems and various physical factors and make the evolution of drought at a large scale elusive. Expanding our knowledge in this regard would enhance our capacity to predict drought cascades and refine global hydrological and land surface models. This advancement is crucial for better understanding the droughts' evolution in the water cycle,

40   improving the identification and attribution of cascading droughts, and enhancing global hydrological and land surface models, which is imperative for effectively forecasting and managing the systematic risks associated with drought in the context of global warming.

    Common methods mainly rely on the point-point or region-region relationship of the drought index to detect the drought cascades (Apurv et al., 2017; Barker et al., 2016; Farahmand et al., 2021; Geyaert et al., 2018) and do not consider the dynamic

45   spatial motion over time. For example, Sutanto et al. (2020) consider the sequence of at least two hazards within each geographic grid, uninterrupted by a zero-hazard day, to be a cascading event to study the occurrence pattern of heatwaves, droughts and wildfires at the pan-European scale. Farahmand et al. (2021) targeted the four most significant drought events in the four fixed regions of the US and investigated the cascading drought phenomenon involving precipitation, runoff, soil moisture, streamflow and groundwater through their drought index variation over time at the unified regional scale. However,

50   the drought index variation in a fixed regional scale cannot reflect the dynamic spatiotemporal nature of drought progression in the real world.

    The identification of three-dimensional drought events by characterizing dynamic spatiotemporal continuous motion is introduced in recent studies (Diaz et al., 2020; Liu et al., 2020; Zhou et al., 2019), which is able to detect more drought events at moderate and small spatial scale. For example, Yoo et al. (2022) found that more monthly droughts in 2007 led to long-term

55   droughts in 2008 in Central Asia, which had not been observed before. Therefore, ignoring the temporal variability of drought areas can lead to an underestimation of the probability and occurrence of droughts (Xu et al., 2015), which can further lead to failure to detect cascading phenomena and miscalculation of large-scale droughts cascade. Some studies have started to introduce dynamic spatiotemporal movement in identifying the connection between two types of droughts (Jiang et al., 2023; Liu et al., 2019a). For instance, Liu et al. (2019a) paired two types of drought events by setting the temporal-spatial overlapping

60   threshold to establish the causal mechanism between them at the catchment scale. Jiang et al. (2023) adopted this approach and used machine learning methods further to examine the propagation possibility of precipitation to ecological droughts. In

the real world, the complexity of coupled and interdependent feedback loops across multiple systems leads to variations in droughts at different spatiotemporal scales, resulting in overlaps that cannot be predetermined within the drought cascade.

Additionally, the basic idea in existing research is to establish the pointwise correlation between the two types of droughts using the standardized hydrological drought index and meteorological droughts at various long-term time scales, by which the time delay among the different droughts could be recognized (Barella-Ortiz and Quintana-Segui, 2019; Barker et al., 2016; Geyaert et al., 2018; Van Loon et al., 2012). However, global warming has sped up the drought intensification rates and triggered the global transition from conventional droughts to more flash droughts (Yuan et al., 2023). The coarse temporal resolution is inadequate for understanding the wicked problems of rapid temporal-spatial transitions during cascading processes that unfold over short-term scales (Bachmair et al., 2015), particularly for flash droughts.

To fill the above-mentioned gaps , this study introduces a novel approach that considers the nature of the dynamic space-time progression in complex drought systems. An identification technique based on spatiotemporal motion similarity was adopted to determine and characterize cascading drought events across multiple systems. Comparing to existing methods, this approach could detect the dynamic space-time cascading connection, utilizes high temporal resolution data and eliminates the need for predefined spatiotemporal overlap thresholds. This method was applied in Central Asia which is a typical arid/semi-arid region. Despite a long history of frequent drought occurrences, the emergent pattern of the drought cascades in CA has not been studied yet. To this end, we employed the proposed method to identify the emergent pattern of the drought cascades in CA and explore their features, including the number of systems involved, temporal order, and total severity. Besides, four characteristics (intensity, severity, duration, and area) of the single drought event are investigated to explore the drought evolution during the cascading progression. This paper is structured as follows: Section 2 provides a brief overview of the geographic information of CA and describes the datasets used in this work and the procedure for identifying the cascading drought events. The results of the proposed approach and the comprehensive analysis are presented in Sections 3 and 4, respectively. Finally, the conclusions are presented in Section 5.

2 Data and method

85 **2.1 Study area**
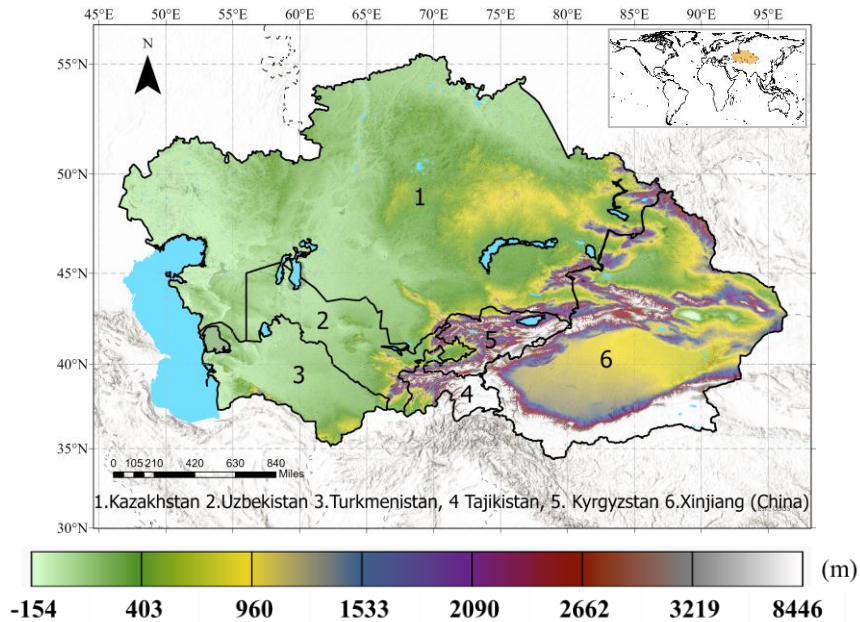
Figure 1. The topography of Central Asia.

We used the definition of the geographical scope of Central Asia by (Hu et al., 2018) as the spatial domain of this study area, namely the north-western regions of China (Xinjiang region), the five countries of the former Soviet Union: Kazakhstan,

90 Kyrgyzstan, Tajikistan, Turkmenistan, and Uzbekistan. Located in the centre of Eurasia and far from the ocean, CA is a typical arid and semi-arid region, often experiencing long-term rainfall deficits and having a variable topography. Figure 1 shows that the topography descends from the eastern mountain ranges to the western steppe region. The Tianshan Mountains, the Pamir Plateau, and the Tarim Basin dominate the terrain and contribute to the region of the eastern alpine and arid desert climates (Xinjiang, Kyrgyzstan, and Tajikistan). The western and central areas are dominated by lower elevations (e.g., Caspian

95 depression), characterized by extensive temperate grassland and shrubland (steppe) zones. This topography results in significant temperature and precipitation gradients from north to south and lowlands to mountains (Beck et al., 2018). The complex interplay between the variable topography and frequent precipitation deficits (Hu et al., 2018; Spinoni et al., 2019) leads to a fragile state within the terrestrial environment, creating conditions conducive to drought events (Guo et al., 2019).

2.2 Datasets

100 In this study, precipitation (PCP) droughts, evapotranspiration (ET) droughts, Runoff droughts, and root zone soil moisture (SM) droughts in the water cycle are investigated to identify and characterise the drought cascades across four types of systems, namely the atmosphere, hydrosphere, biosphere, and soil layer. The datasets used in this study cover the time window from

January 1st, 1980, to December 31st, 2007. The datasets used in this study were standardized to a daily resolution and a spatial resolution of 0.25 degrees. The details of the dataset information are provided below.

105   **Precipitation:** APHRODITE (Asian Precipitation—Highly Resolved Observational Data Integration Towards Evaluation of Water Resources) is the long-term continental-scale daily product with a high spatial resolution for the Asian region. This dataset contains interpolated data from more than 6000 rain-gauge observations in Asia by the distance-weighting method (Yatagai et al., 2012). APHRODITE has been widely used as the benchmark dataset to evaluate the performance of different remote sensing products in various regions throughout Asia (Guo et al., 2017; Guo et al., 2015; Iqbal and Athar, 2018; Jamandre and Narisma, 2013).

110   **Evapotranspiration:** Evaporative Deficit, as the result of actual ET (AET) subtracting potential ET (PET), is the standard direct input of the ET-induced drought index. The potential and actual ET derive from the GLEAM v3.5a project (Global Land Evaporation Amsterdam Model Version 3), have been extensively used to identify drought due to its high temporal-spatial resolution and robust performance (Jiang et al., 2021; Peng et al., 2020). GLEAM calculates the PET with the Priestley-Taylor equation using ERA5 net radiation and air temperature (Miralles et al., 2011b). AET is converted from PET using a multi-layer water-balance algorithm by considering net precipitation (precipitation minus interception loss) and snowmelt (Martens et al., 2017). This dataset has been validated through the FLUXNET global network of micrometeorological flux measurements under various climatic and vegetation situations (Miralles et al., 2011a).

     Root Zone Soil Moisture: Root zone soil moisture is obtained from the GLDASv2.0-Noah dataset ensembles (Sheffield et al., 2006). The daily soil moisture used in this study is the average value of raw data at a 3-hour resolution each day. The soil module of the GLDAS-Noah model comprises four layers, namely 0-10, 10-40, 40-100, and 100-200 cm. The depth of the root zone area depends on the vegetation type. Among the drought recognition ability of remote sensing products, the GLDAS-Noah dataset demonstrated greater capability in detecting drought occurrence over the vegetated region and bare area (Liu et al., 2019b; Ma et al., 2019).

125   **Runoff:** Runoff is the average value of total surface runoff (Q_{total} = surface runoff + subsurface runoff) from seven state-of-the-art global hydrological models' outputs (DBH, H08, LPJmL, MATSIRO, PCR-GLOBWB, VIC, and WaterGAP 2). These data are from ISIMIP2a (Inter-Sectoral Impact Model Intercomparison Project) and forced by the meteorological data from the Watch Forcing Data ERA-Interim (WFDEI) under the 'varsoc' scenario, often used as the validation dataset to evaluate the uncertainty of novel historical runoff reanalysis datasets (Ghiggi et al., 2019). The runoff data at 0.5° resolution was interpolated into 0.25° by the nearest neighbour method in this study.

2.3 Methodology

The approach proposed here is summarised in three parts (Fig.2). The three-dimensional (3D) single drought event is identified in section 2.3.1 based on the continuously dynamic space-time motion. In section 2.3.2, we integrated the different types of single drought events with similar space-time motion to form the cascading drought event. The features of single drought

135   events and cascading drought events focusing on this study were introduced in 2.3.3. As precipitation deficits are generally considered as the initiation of droughts, PCP droughts are considered the commencement of a cascading drought event in this study.
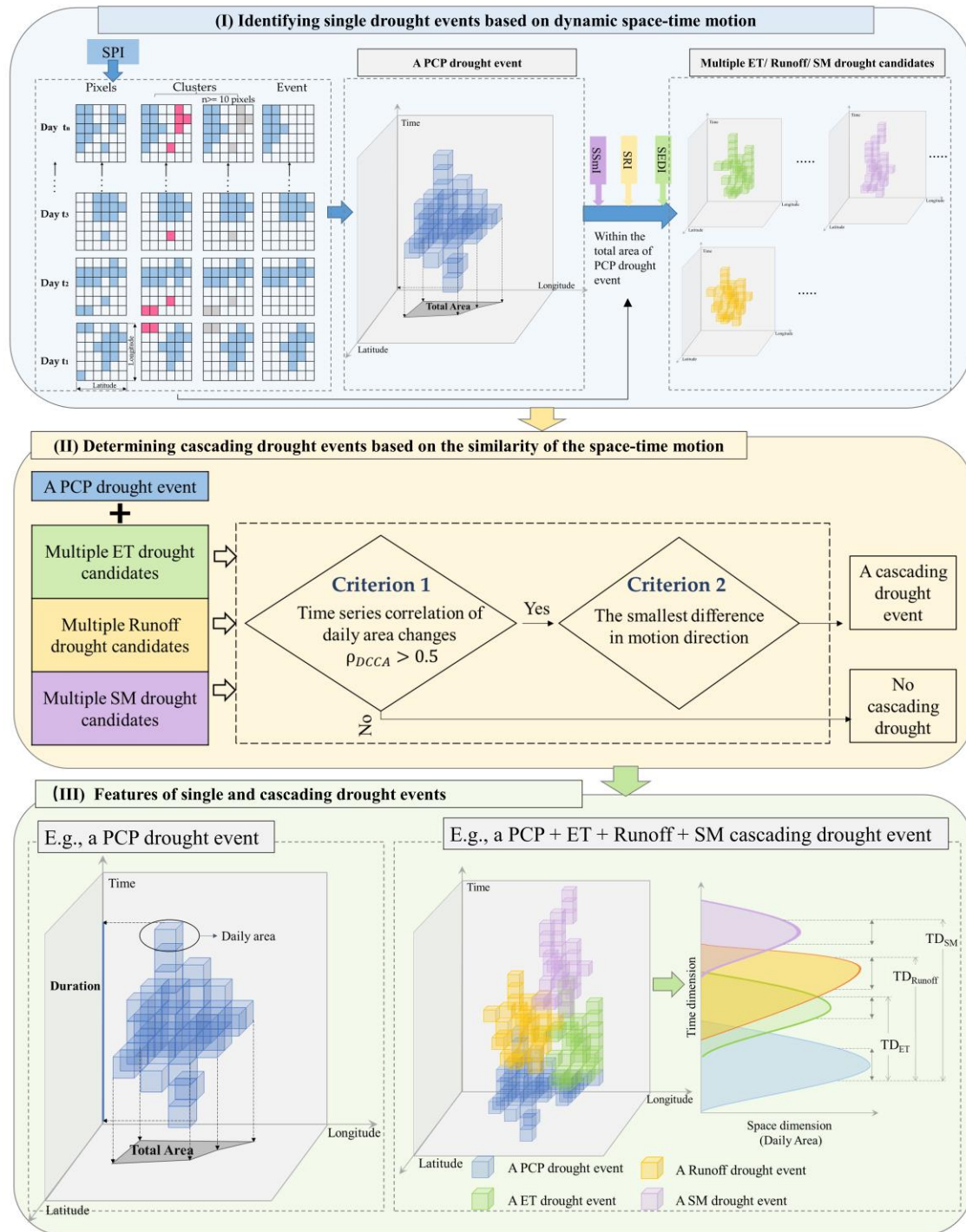
Figure.2. Schematic diagram of methodology detecting the multiple-system cascading event from the space-time dimension

2.3.1 Identifying single drought events based on the dynamic space-time motion

Here, a single 3D drought event is defined by space-time continuum motion to account for the spatial variations in drought development, the approach including the definition of 1) drought pixels (1D, function of time), 2) drought clusters (2D, function of latitude and longitude), and 3) drought events (3D, function of time, latitude, and longitude). The PCP drought event was identified based on these three steps. Within the total area of each PCP drought event, the above three steps were repeated to identify its ET/Runoff/SM drought candidates. The detailed detection approach is as follows.

Step 1: Drought pixels. The Standardized Drought Analysis Toolbox (SDAT) were used to determine drought pixels that only considered time dimensions (Farahmand and AghaKouchak, 2015). The standardized indices (SIs) of one hydrological component were calculated at a daily time scale with 30 days accumulation period. The sum of the corresponding variable for 30 days was compared with the same day on a one-year return period throughout the study period to get the ranking position i. Then, the i value and overall sample size n is the input to the formulation. Four drought indices are employed in this study to represent the crucial drought processes in the water cycle, namely the Standardized Precipitation Index (SPI) (McKee, 1993), the Standardized Evapotranspiration Deficit Index (SEDI) (Vicente-Serrano et al., 2018), the Standardized Soil Moisture Index (SSmI) (AghaKouchak, 2014), and the Standardized Runoff Index (SRI) (Shukla and Wood, 2008). The Weibull non-exceedance probability calculated the centre of probability mass of multiple zeros results to compensate for the non-negligible error from long-zero rainfall and runoff period and get more statistically meaningful SI values. To this end, the SPI and SRI are calculated by Weibull non-exceedance probability (Stagge et al., 2015) and empirical Gringorten plotting position (Farahmand and AghaKouchak, 2015). The SEDI and SSmI only are computed by the empirical Gringorten plotting position. Finally, we could get four kinds of SI_s for each cell daily throughout the study period. The cells with the values lower than -1 are defined as drought pixels (Peng et al., 2020).

$$p(x_i) = \begin{cases} \frac{i-0.44}{n+0.12} & for \; x > 0 \\ \frac{n_0+1}{2(n+1)} & for \; x = 0 \end{cases} \tag{1}$$

i: the ranking position of accumulation value; n: the sample size of all accumulation values within each pixel.

Step 2: Drought clusters. Adjacent drought pixels with common sides were clustered each day to form spatially contiguous 2D drought clusters (latitude and longitude) for each day. We used 10 pixels as the minimum spatial area threshold for a drought cluster in this study (Andreadis et al., 2005). Most drought clusters are irregular polygons. The daily drought cluster determined the daily area of a drought event.

Step 3: Drought events. After all drought clusters were generated throughout the study area over the study period, the 2D drought clusters on consecutive two days were linked together to form a 3D drought event (latitude, longitude, and time). The linking rule is to check if there is an overlapping pixel at adjacent time steps. If there is an overlapping area, the

clusters are considered one single event. This procedure ended when no following spatial overlapping cluster existed on the next time step. The tree traversal was utilized to ensure a daily cluster only belong to one drought event. All drought clusters would be classified as numerous individual assemblies after being traversed. The time step spanned by each assembly was characterized as duration. Considering the recent developments of flash droughts across the world (Basara et al., 2019; Christian et al., 2021), we adopt 15 days as the minimum duration threshold following the general definition of flash drought that lasts at least two weeks (Pendergrass et al., 2020), to incorporate the monthly and sub-monthly droughts. Hence the independent assemblies over 15 days were kept and viewed as separate drought events. This step allows us to identify each drought event's onset, end time, and track its spatial drought movement path (see Fig.2).

2.3.2 Determining cascading drought events based on the similarity of the space-time motion

This section aims to identify the cascading drought event for a PCP drought from multiple candidates of ET, Runoff, and SM droughts based on the similarity rule of the space-time motion. The steps outlined in this section aim for a single PCP drought event, which will be replicated independently for all PCP droughts to identify all the associated cascading drought events. As the selection process is identical for all ET, runoff, and SM drought candidates, the "D$_{candidate}$" will be used collectively to refer to all three types of drought candidates in the following description. The two criteria employed in determining the cascading drought events are elaborated below. Based on two criteria, the ET / Runoff / SM droughts are determined for each PCP drought to form the multi-system cascading drought event. Notably, there is only one drought event for each type in each cascading drought event. Furthermore, existing research emphasizes that the propagation of drought impacts from precipitation deficits to hydrological droughts has been proven to be less than 12 months (Ding et al., 2021). To this end, the threshold from the PCP drought onset day to 365 days was applied as the temporal boundary in assessing the sequential cascading relationship of ET/runoff/SM droughts.

Criterion 1:   Time series correlation of daily area changes of the PCP drought event and drought candidates

The first criterion is the time series correlation of daily area changes of multiple D$_{candidate}$ $\{y'_{Dcandidate}\}$ and their corresponding PCP drought event $\{y_{PCP}\}$. The time series in the real world usually presents autocorrelation and high-degree nonstationary, which could cause spurious correlations. Therefore, the correlation in this study is estimated by Detrended Cross-Correlation Analysis (DCCA) (Podobnik and Stanley, 2008; Zebende, 2011) and Detrended Fluctuation Analysis (DFA) (Peng et al., 1994; Peng et al., 1992). It is particularly useful when analysing nonstationary and autocorrelated data.

1) Compute two integrated signals of two cross-correlated time series with equal length N: $\{y_i\}$ and $\{y'_i\}$. k =1, 2, 3… N.

$$Y_k \equiv \sum_{i=1}^{k} y_i \tag{2}$$

$$Y_k{}' \equiv \sum_{i=1}^{k} y'_i \tag{3}$$

2) Divide each time series into N-n overlapping boxes containing n+1 values. The ordinate of a linear least-squares fit of each time series segment is the 'local trend': $\tilde{Y}_{k,i}$ and $\tilde{Y}_{k,i}'$ $(i \leq k \leq i + n)$. The difference between the original walk and the local trend is defined as the 'detrended walk.'

3) The integrated signal Y_k is detrended by subtracting the local trend $\tilde{Y}_{k,i}$ in each box.

$$f_{DCCA}^2(n, i) \equiv \frac{1}{n-1}\sum_{k=i}^{i+n}(Y_k - \tilde{Y}_{k,i})(Y_k' - \tilde{Y}_{k,i}') \tag{4}$$

4) The $F_{DCCA}^2(n)$ for the time signal is counted by:

$$F_{DCCA}^2(n, i) \equiv \frac{1}{N-n}\sum_{i=1}^{N-n} f_{DCCA}^2(n, i) \tag{5}$$

The indicator, DCCA cross-correlation coefficient (ρ_{DCCA}), is defined as the ratio between the detrended covariance function F_{DCCA} and the detrended variance function F_{DFA} (see Eq. (6)). ρ_{DCCA} is a dimensionless coefficient that ranges between $-1 \leq \rho_{DCCA} \leq 1$. When $\rho_{DCCA} = 1$ means perfect cross-correlation; $\rho_{DCCA} = 0$ means no cross-correlation; $\rho_{DCCA} = -1$ means perfect anti cross-correlation. In this study, we believe that the effective correlation exists when the coefficients higher than 0.5 (Zebende, 2011). The SI$_{candidate}$ with ρ_{DCCA} below 0.5 in the correlation coefficients assemblies will be removed. This step determines the system number of the final cascading drought event. For example, if there are only ET drought candidates is correlated with PCP droughts with $\rho_{DCCA} > 0.5$ and no SM and Runoff droughts candidates meet this threshold, the cascading drought event is the two-system cascading drought event as there is only two types of droughts.

$$\rho_{DCCA} \equiv \frac{F_{DCCA}^2}{F_{DFA\{y_{PCP}\}}F_{DFA\{y'_{Dcandidate}\}}} \tag{6}$$

Criterion 2:   Difference of motion direction between the PCP drought event and its drought candidates

After filtering by the first criterion, the second criterion is the difference of motion direction between PCP and multiple D$_{candidate}$. Dominant movement direction was recognized as the two geographical angles reflecting in drought movement trajectory: 1) the geographical angle from the onset cluster centre to the peak cluster centre; 2) the second is from the peak cluster centre to the termination cluster centre. The centre was calculated by the arithmetic mean of the longitude and latitude of each drought cluster. The schematic of the trajectory of a drought event is displayed in Fig. 3. The drought event, with the minimum direction difference relative to the PCP drought event, is identified to form the final cascading event.
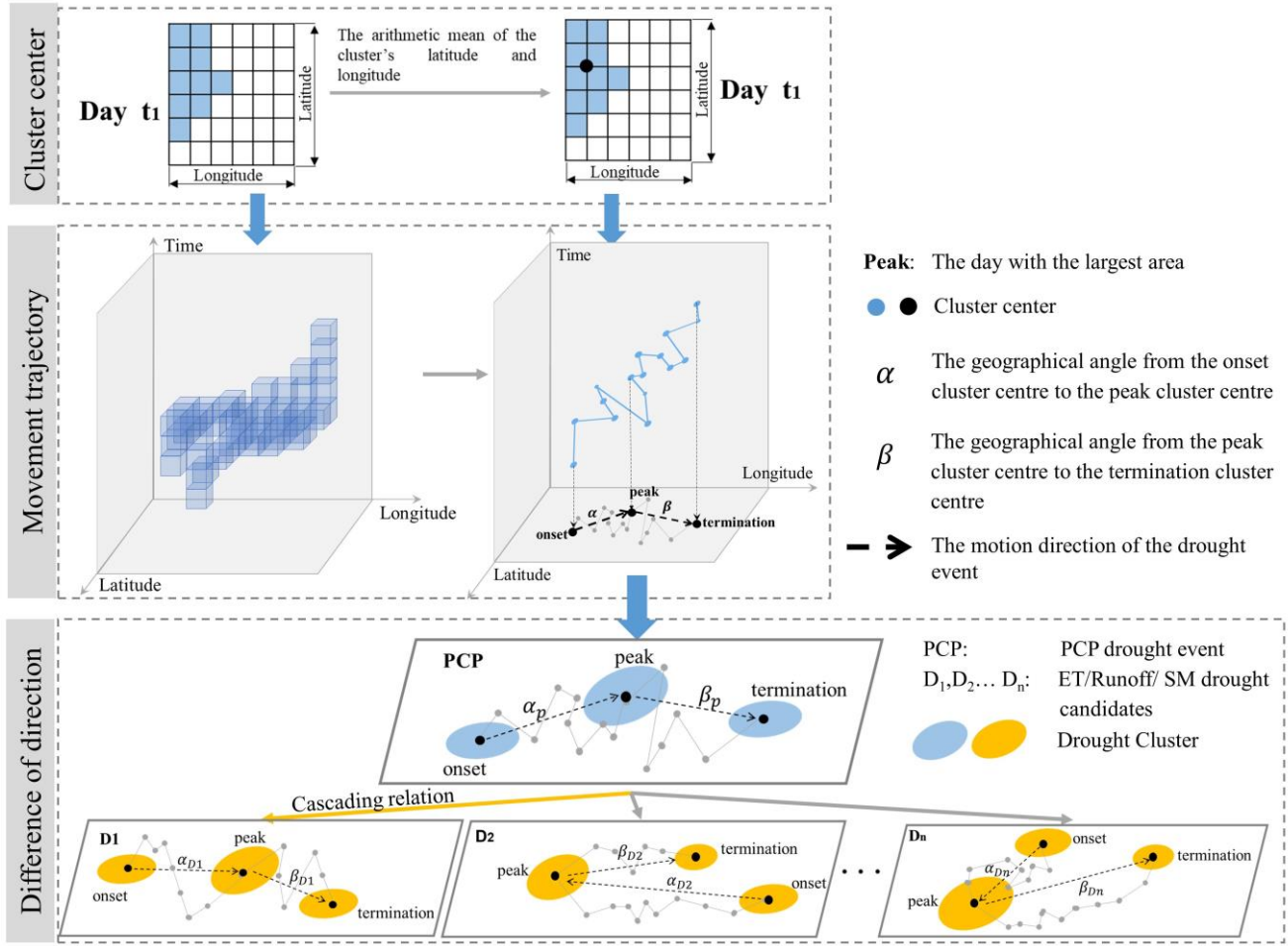
Figure 3. The schematic diagram for identifying the motion direction of a single drought event and a cascading event according to the metric of similarity in spatial motion

2.3.3 Features of single and cascading drought events

First, four characteristics of each single drought event within a cascading event are evaluated, including 1) duration, 2) intensity, 3) severity, and 4) total area. The temporal span of an event was defined as the duration of a drought event T. Intensity and severity were defined in Eq. (8) and Eq. (9). Total Area is the number of all pixels of daily drought clusters but overlapped areas of clusters at different day only count once.

$$I_j(t) = SI \tag{7}$$

$$I = \frac{1}{T}\sum_{t=1}^{T}\frac{\sum_{j=1}^{N}I_j(t)}{N} \tag{8}$$

$$S = \sum_{t=1}^{T}\sum_{j=1}^{N}I_j(t) \tag{9}$$

where $I_j(t)$ is the intensity at day t in grid cell j, namely standardized drought index calculated in section 2.3.1.1. N is the number of grid cells in the cluster at time t. I denotes the intensity of a drought event, which is the mean intensity of all drought cells during the drought's duration. S is the drought severity, the accumulation of $I_j(t)$ along with duration T over area.

Second, the number of systems involved, temporal order, and total severity were used to categorize these cascading drought events in this study. All cascading drought events with the same number of systems involved and temporal order were categorized as the same cascading drought pattern. The total occurrence of cascading patterns was calculated as the event number per cascading pattern divided by the total number of cascading drought events (508) from 1980–2007 across Central Asia.

Table 1 Cascading drought patterns considered for analysis in Central Asia

Number	Combinations of single droughts	Number of systems involved
0	PCP	No cascading drought
1	PCP + ET	Two-system cascading drought pattern
2	PCP + Runoff	
3	PCP + SM	
4	PCP + ET+ Runoff	Three-system cascading drought pattern
5	PCP + Runoff +ET	
6	PCP + ET + SM	
7	PCP + SM + ET	
8	PCP + Runoff + SM	
9	PCP + SM + Runoff	
10	PCP + ET + Runoff + SM	Four-system cascading drought pattern
11	PCP + ET + SM + Runoff	
12	PCP + Runoff + ET + SM	
13	PCP + Runoff + SM + ET	
14	PCP + SM + ET + Runoff	
15	PCP + SM + Runoff + ET	

The 15 cascading patterns in Table 1 were identified in this study. For example, PCP+ET+SM denotes the order of occurrence starting with precipitation droughts, followed by the ET droughts, and ending with SM drought event. Furthermore, the number of single drought events in a cascading event determines the system number, which also denotes the systems involved in the cascading drought events. For example, PCP + SM + ET + Runoff belongs to the four-system cascading drought event, as it includes four single drought events associated with four systems. The temporal order is predominantly determined by the time delay (TD) between PCP droughts and ET/Runoff/SM droughts. It is computed by measuring the actual time lag between similar spatial and temporal movement components (namely $p_{DCCA} > 0.5$) of PCP droughts and the corresponding runoff / ET / SM droughts (Fig. 2).

250   In addition, we employed the total severity of the cascading drought event to evaluate the systematic severity. The total severity (S_{total}) of the cascading drought event was the cumulative value of the severity of all included single drought events; see Eq. (10), where p is the number of single drought events within a cascading drought event. The number of systems involved is the upper limit of individual drought event number (p) in each cascading drought event.

$$S_{total} = \sum_{p=1}^{System} S_p \tag{10}$$

255 **3 Result**

3.1   Patterns and occurrence of cascading drought events

This study identified 503 cascading drought events. Among these, four-system cascading drought pattern (51.38%) occurred more frequently than the three-system (37.99%) and two-system (9.64%) cascading drought pattern across the study region (Fig. 4). This higher prevalence of four-system cascading patterns suggests that PCP, ET, runoff, and SM droughts tend to
260 occur in a consecutive manner instead of in isolation. Notably, the cascading drought patterns that occurred with a frequency greater than 10% were PCP + ET + Runoff (17.52%), PCP + Runoff + ET (16.93%), and PCP + ET + Runoff + SM (12.40%). In contrast, the PCP + SM cascading pattern, which is associated with root zone soil moisture, was the least frequent cascading pattern, accounting for less than 0.4% during the study period. ET droughts exhibited a shorter average time delay, with a higher concentration of data points in the lower quartile of the violin boxplot (Fig. S1). In contrast, SM droughts have a longer
265 average time delay, with a greater concentration of data points in the upper quartile of the violin boxplot. This evidence suggests that ET droughts occur predominantly as the initial system of the drought cascade following PCP droughts, while Runoff and SM droughts tend to follow sequentially as the second and third positions, respectively.
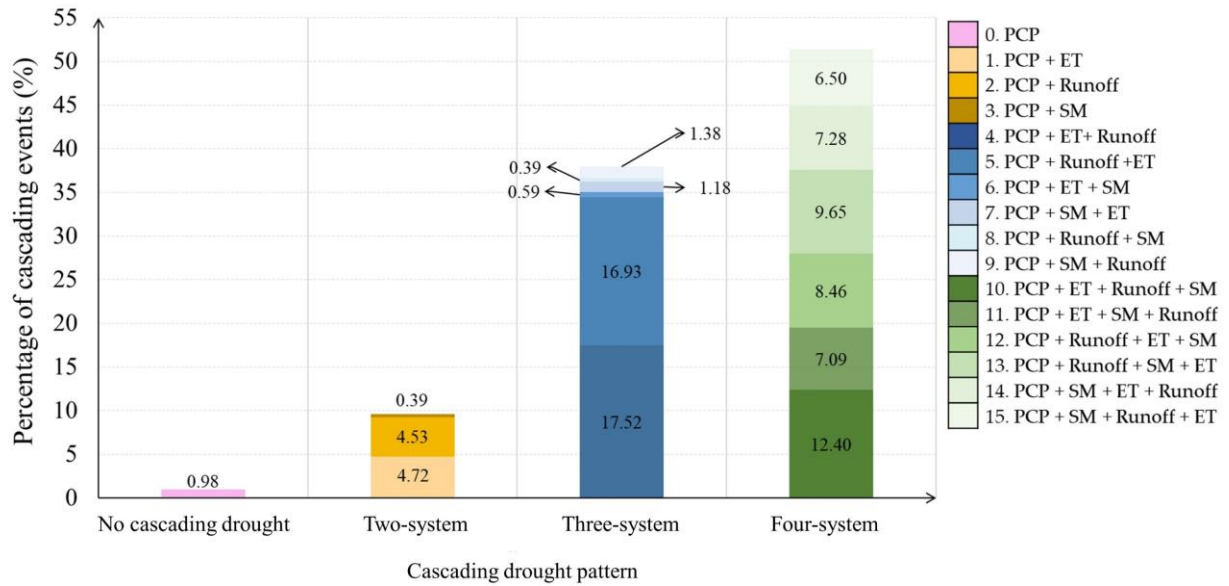
Figure 4. Total occurrence of all cascading drought patterns

3.2   Characteristic evolution within the cascading drought event

Notable characteristic evolution in duration, area, and severity is observed among PCP, ET, Runoff, and SM droughts during the cascading process. The duration of droughts was significantly extended when the droughts progressed from the atmosphere to the terrestrial system. Specifically, the duration of PCP droughts is the shortest among the four types of droughts. In contrast, SM droughts involving the root zone soil layer exhibit the most extended duration (Fig.5a) in all cascading drought patterns. For the ET, Runoff, and SM droughts occurring in the terrestrial system, the area of ET droughts is significantly greater than that of Runoff droughts. The affected area of SM drought is consistently the smallest among all cascading patterns (Fig.5b). Regarding severity (Fig.5c), SM droughts exhibit the lowest average severity among the three types of cascading droughts occurring on the land surface in three-system and four-system cascading patterns. But several extremely severe SM droughts exceed the upper threshold of severity for ET and Runoff droughts.

The upper limits regarding the duration, area, and severity of PCP, ET, Runoff, and SM droughts are significantly higher in four-system cascading patterns compared to the same drought type in two-system and three-system cascading patterns (Fig. 5), indicating that the high-system cascading pattern consists of more pronounced drought events. For example, all droughts in two-system cascading patterns last less than 365 days, while in three-system and four-system cascading patterns, drought events persisting for more than 365 days are much more (Fig. 5a). These findings suggest that when single long-term droughts with markedly severe distribution over large areas are observed, the high-system cascading drought event will likely to accompany.
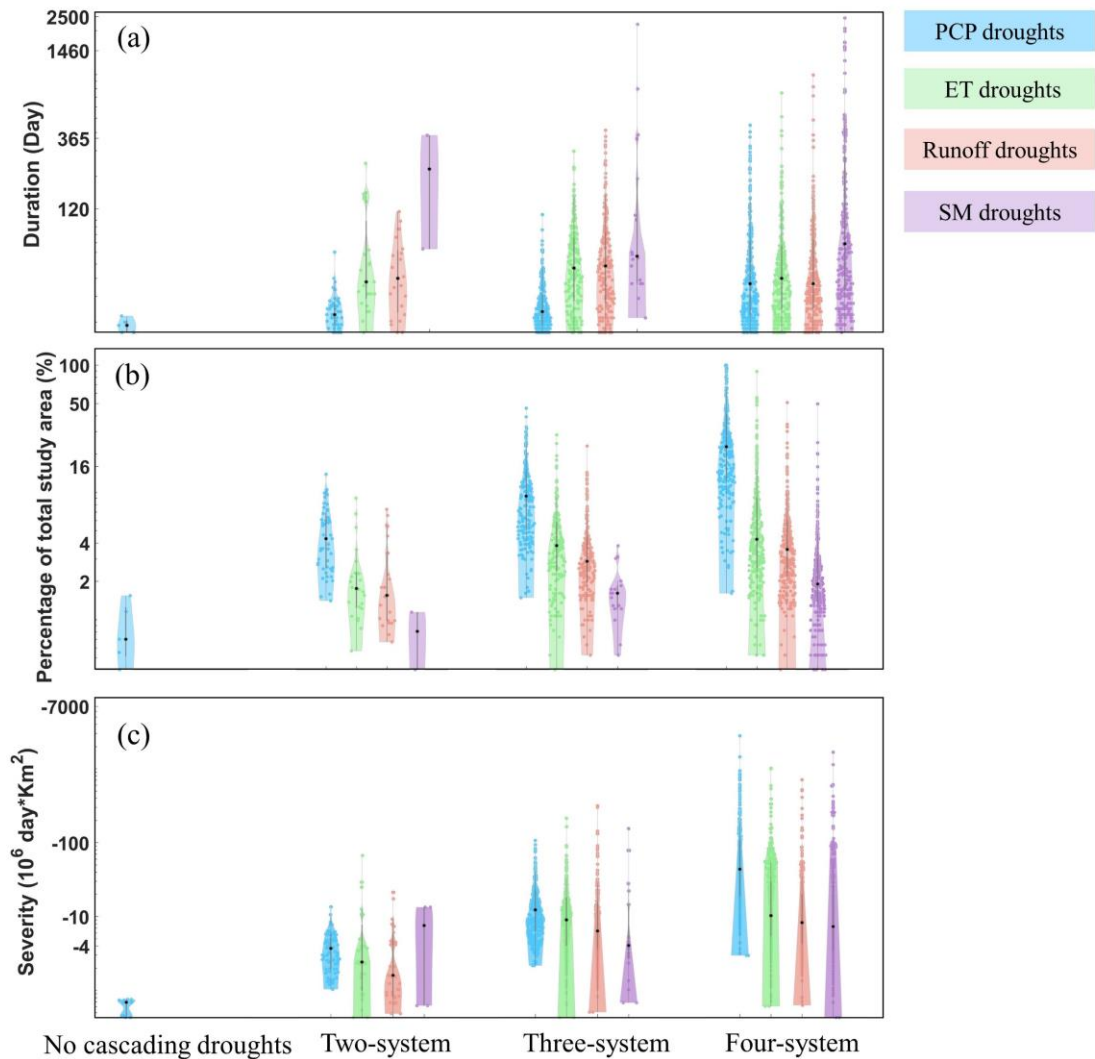
Figure 5: The duration, area, and severity of drought events in the cascading drought patterns. The bandwidth denotes the density of the values quantified by the kernel density estimate. The black circle in the violin plot indicates the median value

3.3 The 9 most severe cascading drought events

Based on the total severity, the 3 most severe cascading drought events for different numbers of systems invovled are identified and the corresponding drought characteristics are listed in Table 2. As shown, the total severity of three top cascading events in the two-system cascade are from -11.46 to -32.87*10^6 Day*km^2, remarkably lower than that in three-system (-78.15 to -127.84 *10^6 Day*km^2) and four-system cascading event (from -2038 to -925.78*10^6 Day*km^2). The higher total severity of cascading events with more systems involved suggests that the increased systematic risk when the cascading drought event involves more systems.

The most severe cascading drought event is the PCP+Runoff+ET+SM (No.7) in the four-system cascading pattern. This cascading event commenced from the PCP drought on 09-Dec-2006 and terminated by the end of PCP droughts on 29-Dec-2007, lasting for over 12 months and spanning 99.8% of the study area. During the same period, the Runoff drought emerged on 01-Jan-2007 and terminated on 13-May-2007, lasting 133 days. The ET drought followed the Runoff drought and appeared in the summer lasting from 24-Jun-2007 to 29-Jul-2007. The SM drought occurred at the latest and persisted for 50 days with the smallest affected area. The severe drought event that occurred in 2007 coincided with the findings of Yoo et al. (Yoo et al., 2022). The Food and Agriculture Organization (FAO) has also documented substantial damage to the agriculture sector due to the drought event affecting Turkmenistan, Tajikistan, and Kyrgyzstan in 2007 (Patrick, 2017).

As the cascading connection in this study is identified by the spatial-temporal dynamic movement rather than fixed spatiotemporal overlapping thresholds, there is not always a temporal overlapping pattern in all cascading drought events. For instance, in the No.2 cascading drought event, the PCP drought lingers from 19-Jul-2002 to 06-Aug-2002, while the ET drought commences on 26-Jul-2002, during the middle of the PCP's persistence period. In contrast, in the No.5 cascading drought event, the PCP drought occurred during the spring of 1997, lasting from 22-Mar-1997 to 09-Apr-1997, and does not exhibit temporal overlap with the subsequent SM drought from 22-June-1997 to 17-Jul-1997.

Table 2. Top 3 cascading drought events in two-system, three-system and four-system cascading drought pattern according to the total severity

Type	Number	Pattern	Drought type	Onset	Termination	Severity (10^6 Day*km^2)	Area (10^5 km^2)	Duration (Day)	Maximum intensity	Total severity (10^6 Day*km^2)
Two-system cascading pattern	1	PCP+ET	PCP	'15-Aug-2001'	'19-Sep-2001'	-2.45	2.34	36	-1.4	-32.87
			ET	'03-Jan-2002'	'13-May-2002'	-30.43	2.28	131	-2.06	
	2	PCP+ET	PCP	'19-Jul-2002'	'06-Aug-2002'	-1.7	1.55	19	-1.77	-13.18
			ET	'26-Jul-2002'	'13-Dec-2002'	-11.48	1.54	141	-1.82	
	3	PCP+Runoff	PCP	'04-Oct-1991'	'26-Oct-1991'	-3.53	2.58	23	-1.53	-11.46
			Runoff	'26-Apr-1992'	'09-Aug-1992'	-7.93	1.71	106	-1.66	
Three-system cascading pattern	4	PCP+ET+Runoff	PCP	'27-May-1983'	'21-Jul-1983'	-5.88	6.88	56	-1.53	-127.84
			ET	'23-Dec-1983'	'20-Jan-1984'	-0.06	0.06	29	-1.58	
			Runoff	'10-Jan-1984'	'09-Feb-1985'	-121.89	6.55	396	-1.84	
	5	PCP+SM+Runoff	PCP	'22-Mar-1997'	'09-Apr-1997'	-3.95	3.05	19	-1.76	-119.16
			SM	'22-Jun-1997'	'17-Jul-1997'	-0.36	0.15	26	-1.3	
			Runoff	'01-Apr-1997'	'24-Mar-1998'	-114.84	2.98	358	-1.99	
	6	PCP+Runoff+ET	PCP	'18-Apr-2005'	'03-May-2005'	-4.51	8.05	16	-1.45	-78.15
			Runoff	'16-Aug-2005'	'03-Sep-2005'	-0.38	0.27	19	-1.59	
			ET	'19-Sep-2005'	'02-Mar-2006'	-73.26	7.03	165	-1.82	
	7		PCP	'09-Dec-2006'	'29-Dec-2007'	-2022.85	63.09	386	-1.87	-2038.82

		PCP+Runoff+ET+SM	Runoff	'01-Jan-2007'	'13-May-2007'	-12.83	4.69	133	-2.04	
			ET	'24-Jun-2007'	'29-Jul-2007'	-2.24	1.03	36	-1.72	
			SM	'10-Nov-2007'	'29-Dec-2007'	-0.89	0.16	50	-1.21	
Four-system cascading pattern	8	PCP+SM+Runof+ET	PCP	'25-Jan-1991'	'10-Aug-1991'	-314.02	51.83	198	-1.75	
			SM	'07-Jul-1991'	'15-Mar-1998'	-1012.44	21.32	2442	-1.7	-1336.31
			Runoff	'21-Oct-1991'	'21-Dec-1991'	-2.05	0.61	62	-1.74	
			ET	'03-Jan-1992'	'12-Jun-1992'	-7.8	1.34	161	-2.04	
	9	PCP+SM+Runoff+ET	PCP	'10-Apr-1984'	'16-Dec-1984'	-406.59	61.74	251	-1.84	
			SM	'17-May-1984'	'09-Jun-1984'	-0.26	0.08	24	-1.55	-925.78
			Runoff	'12-Jul-1984'	'06-Aug-1984'	-0.72	0.35	26	-1.39	
			ET	'24-Oct-1984'	'18-Oct-1986'	-518.21	52.92	725	-1.99	

3.4 Dynamic temporal-spatial progression of all single droughts in a cascading drought event
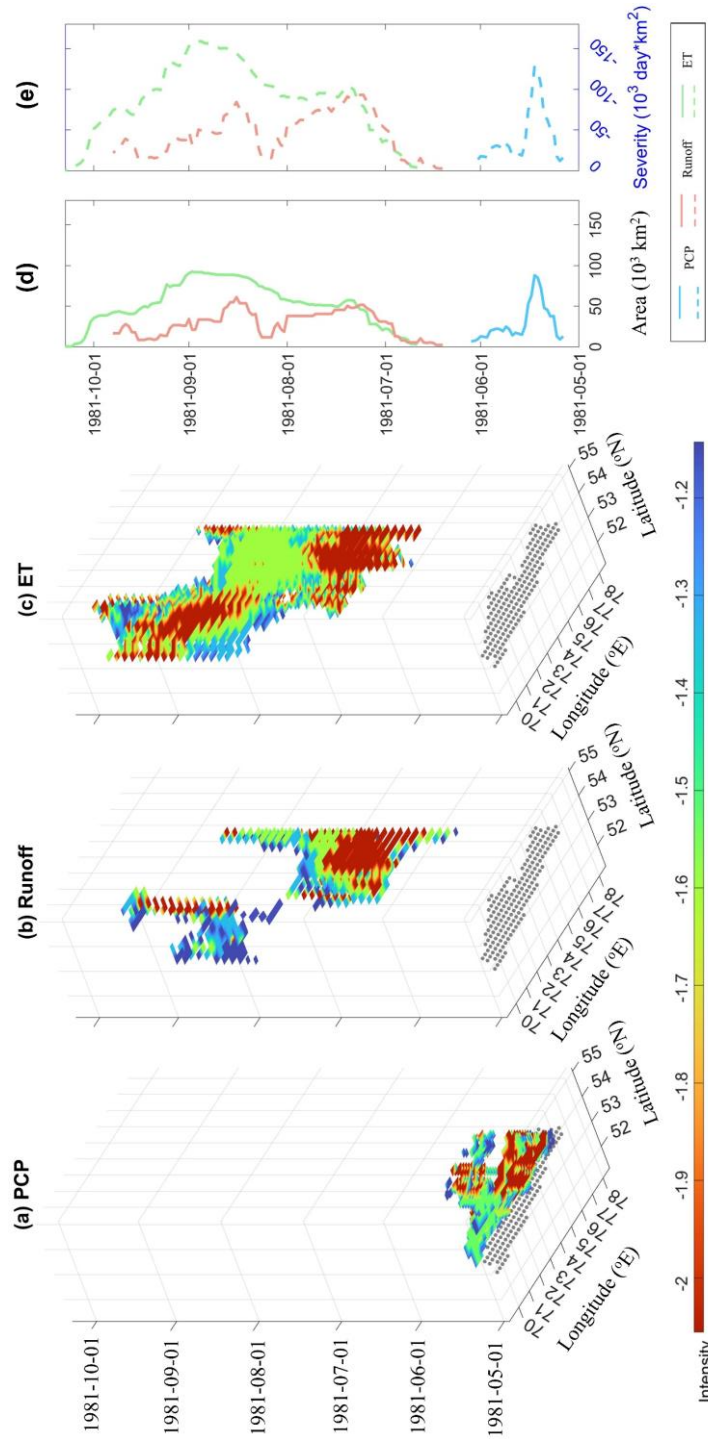
Figure 6. Dynamic temporal-spatial progression of all single droughts in the PCP+Runoff+ET cascading drought event (a) three-dimensional spatiotemporal movement of three single events. The grey area at the bottom is the PCP drought area. The time series of (b) area and (c) severity progression of three single droughts in the cascading drought event.

315

A PCP+Runoff+ET cascading drought event is taken as an example to elaborate the spatial-temporal continuum movement during cascading processes in detail (Fig.6a-c). This cascading event lasted five months, from the onset of the PCP drought on 06-May-1981 to the end of the ET drought on 10-Oct-1981. The affected area spread around the northern region of Kazakhstan, where all single droughts spread east-westwards (Fig.7). The PCP drought developed and decayed rapidly (Fig.6d and 6e)

320   within 30 days. The PCP drought began on 06-May-1981, extended quickly to the peak (88125 km^2) within nine days, and then disappeared within 20 days. Runoff drought and ET drought develop relatively slower than PCP drought. The Runoff drought lasted 105 days, starting on 13-Jun, peaking at 17-Aug (61250 km^2), and terminating on the 25-Sep. The ET drought began on 21-Jun, peaked on the 30-Aug (92500 km^2), and terminated on the 10-Oct.
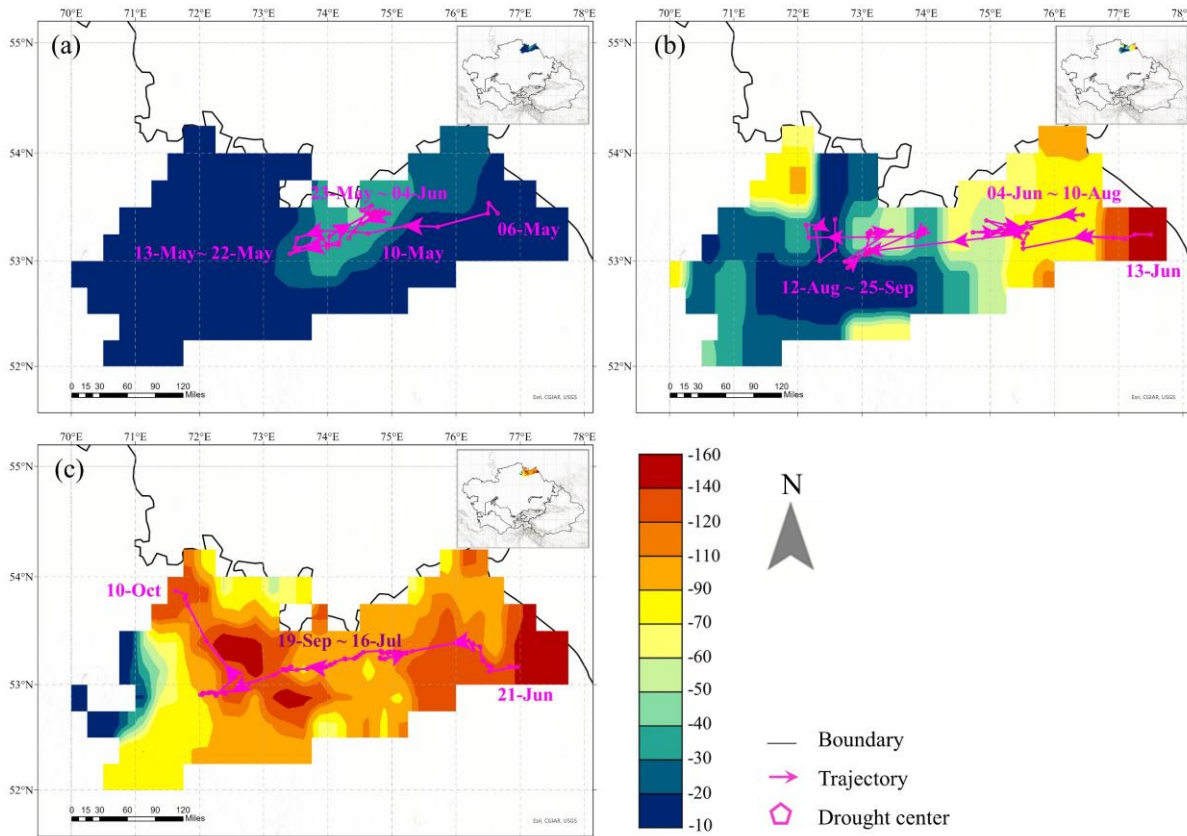
325   **Figure 7: Cumulative intensity and movement trajectory of the (a) PCP drought, (b) Runoff drought, (c) ET drought in PCP+Ruoff+ET cascading drought event.**

3.5 Characteristics of PCP drought could signalize systematic drought risk of cascading events

Cascading drought events, which present a systematic drought risk induced by drought evolution, deserve more attention than the traditional focus on individual droughts due to their higher severity (Fig. 8) and the more dynamic spatial and temporal

330   scope. Traditional approaches to drought assessment have focused primarily on analysing single systems, neglecting the

potential for cascading linkages between different systems, potentially leading to an underestimation of overall drought risk. Some isolated droughts may not be noticeable. However, when multiple hazards are aggregated and occur in conjunction, their combined severity becomes more apparent, leading to more pronounced consequences on the socio-economic system. For example, a single PCP drought of only 30 days, such as the cascading event shown in Section 3.4 (Figs. 6-7), may not be considered a significant drought event. However, when considering the subsequent runoff and ET drought, the cumulative systematic risk of all the droughts included in the cascading drought event must still be considered. Fig 8 shows an apparent increasing trend in total severity as the number of systems increases. CA is dominated by the four-system cascading drought pattern (Fig. 4). This suggests that once the PCP droughts occur, the high systematic drought risk in Central Asia, spreading across the atmosphere, biosphere, hydrosphere and root zone, is likely to emerge. To this end, it is imperative to broaden the scope of drought risk assessments to include cascading hazards to enable the development of comprehensive drought management plans that take into account the magnitude and characteristics of impending disasters (de Brito, 2021).
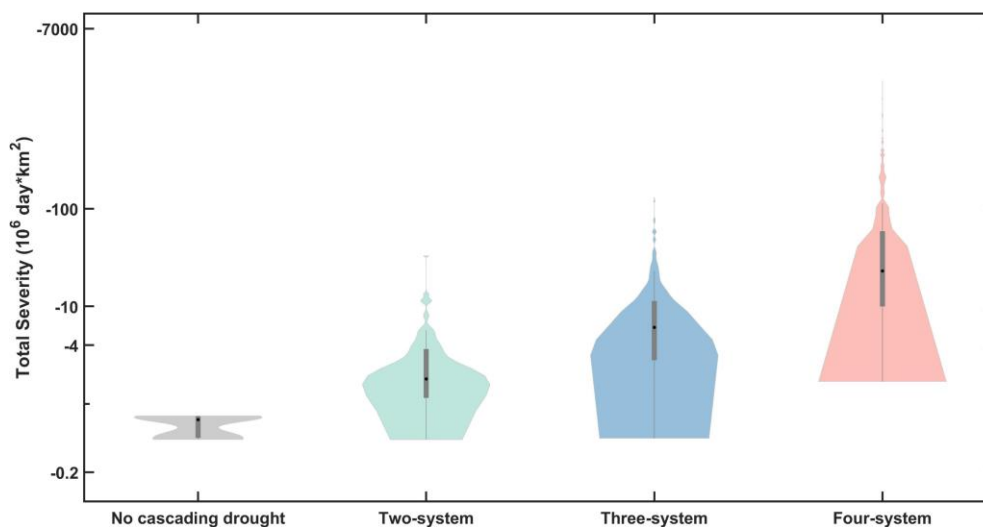
Figure 8: Violin plot of total severity of cascading drought events in different system cascading patterns.

The droughts in terrestrial system identified in cascading drought events, including ET droughts in the biosphere, Runoff droughts in the hydrosphere, and SM droughts in the root-zone soil layer, exhibit a prolonged duration compared to PCP droughts in the atmosphere (Fig. 5). This phenomenon is consistent with the findings of (Jiang et al., 2023), where ecological droughts defined by the drought index including soil moisture and NDVI, persist longer than meteorological droughts defined by SPI. The persistence of ET droughts, Runoff droughts, and SM droughts may be attributed to the fragile ecosystem resilience in Central Asia, which is originally shaped by the arid environment and sparse vegetation cover, leading to desertification risks and poor recovery capability (Jiang et al., 2019). SM droughts have the longest duration, slightest severity, and smallest area relative Runoff droughts and ET droughts (Fig.5), suggesting that the fluctuations in drought signal become smoother and broader when they proceed from meteorology through depth to the root zone soil. This result is consistent with the findings of

existing research (Farahmand et al., 2021; Van Loon, 2015). This phenomenon may be driven by the complex trade-offs between vegetation, groundwater, and human activities that make droughts in terrestrial systems slower, stealthier, and more persistent than droughts in the atmosphere.

As the commencement of the cascading drought event, precipitation has the more readily available data compared to ET, Runoff, and SM. To examine if the PCP single drought events could signify the severity of systematic drought risk, features of PCP drought in the cascading events involving the different amounts of systems were investigated in. Fig. 9. Interestingly, the upper threshold of PCP droughts duration in four-system, three-system, two-system, and no cascading drought patterns corresponds to the types of yearly (420 days), seasonal (101 days), monthly (55 days), and sub-monthly (22 days), respectively. This data implies that there would be a four-system cascading drought event after seasonal PCP drought events lasting longer than 101 days occur. The severity and area of in magnitude in PCP droughts increase as the number of systems increases (Fig. 5), further proved in Fig 9c and 9d. The upper threshold of severity (Fig.9c) in four cascading droughts patterns could reach up to -2022.9, -29.7, -4.7, and -0.76 10^6 day*km^2, whereases that of area percentage is 99%, 30%, 6.5%, and 1.5%, respectively (Fig.9d). The intensity of PCP droughts in four-system cascading patterns is higher than in the other three patterns (Fig.9b). However, the intensity of PCP droughts in the no-cascading drought pattern is higher than in the three-system and two-system cascading drought pattern, and in some cases even higher than in the four-system cascading pattern. However, it may be limited by their short duration and small areas. PCP droughts in the no cascading drought pattern did not form the cascading drought event.

The above result highlights that the characteristics of PCP droughts could serve as indicators of systematic drought risk. Long-term PCP droughts with greater severity and intensity in larger areas are more likely to form extensive cascading droughts across more systems and cause greater systematic risk. Further research is needed to understand the characteristics and underlying mechanisms of moderate and small PCP droughts that trigger cascading drought events with more systems involved.
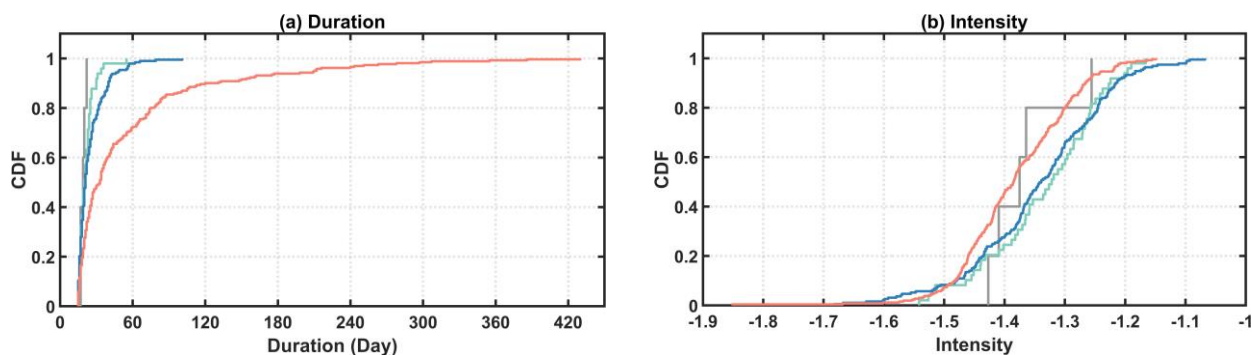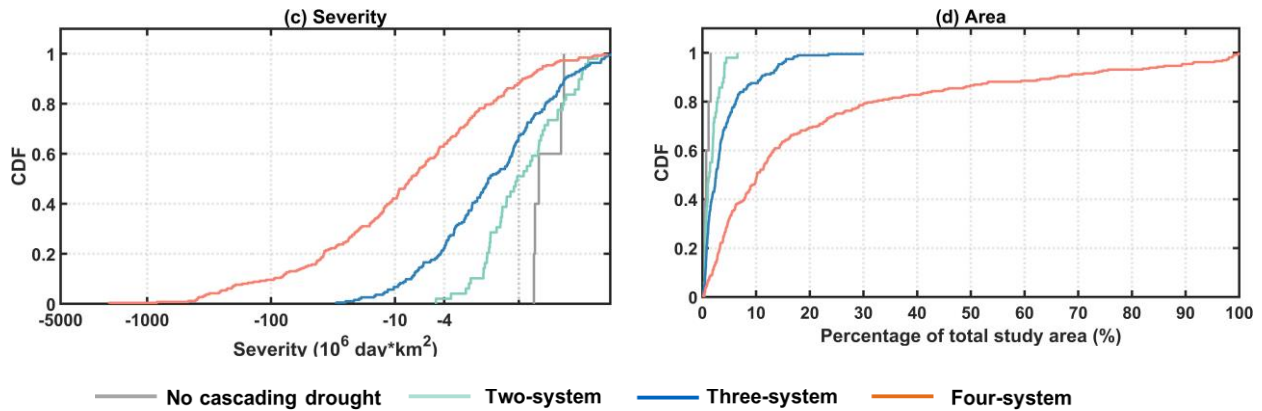
Figure 9: Cumulative distribution plot of the PCP drought features in the cascading drought pattern: a) duration, b) intensity, c) severity, and d) area.

4 Discussion

4.1 Integrated driving effects of energy-limited and water-limited regimes on cascading drought patterns in CA

Multiple cascading drought patterns with mixed temporal order were identified in this study. The result likely reflects the integrated driving effect of the water-limited and energy-limited phases. When at the energy-limited phase, the soil moisture is sufficient and does not regulate the evaporation. During this period, the precipitation deficit might enhance the potential and actual evaporation demand. The cascading drought pattern might present the PCP+Runoff, PCP+Runoff+ET, or PCP+ET+SM. When the water-limited phase begins, PET could continue to increase. However, the increase in AET is no longer sustained and subsequently decreases as soil moisture deficits are limited, during which the evaporative deficit gradually increases and evaporative droughts are exacerbated (Pendergrass et al., 2020). During the water-limited phase, the cascading drought pattern possibly presented as the PCP+SM+ET.

The three most common cascading drought patterns identified in this study are PCP+ET+Runoff, PCP+Runoff+ET and PCP+ET+Runoff+SM. This result could be explained from two aspects. 1) The drought signal in soil moisture only sometimes are detected. 2) Given the more significant evaporative deficits in the water-limited phase, the significant ET droughts signal after PCP droughts shown in the cascading drought pattern indicates the occurrence of cascading droughts under the water-limited phase. This result could be due to three possible reasons. First, the SM data adopted in this study are from the soil layer of 40-100cm. The shrubland and grassland with short roots are the dominant vegetation in the study area (Klein et al., 2012), and their root density is typically concentrated on the 0-40 cm soil layer (Kurc and Small, 2007). It could result in lower vegetation water requirements and less fluctuation of the space-time signal of soil moisture in the deep layer.

Second, the coupling of SM and evaporation raw data might not be reflected by their drought index. The fluctuation in deep layer soil moisture is most stable relative to the precipitation and runoff (Van Loon, 2015). The SM drought index might not recognise declines in SM in the constantly dry region that fluctuates within a small magnitude. Moreover, the spatio-temporal

progression of SM and ET droughts is different. The spatiotemporal progression of SM droughts is the slowest compared to
400 the other three droughts, which is reflected by the fact that SM droughts are the longest in duration and the smallest in the area
(Fig. 5).

Third, the effect of energy-limited regimes could be underestimated in Central Asia. Hsu and Dirmeyer (2023) recognized
most Central Asia as the transitional and energy-limit regime. Yuan et al. (2023) found that around 30%-50% of soil moisture
drought events in CA are flash droughts possibly induced by the precipitation deficit and increased evapotranspiration at the
405 energy-limited phase. This could be presented as the PCP+ET+SM or PCP+ET+Runoff+SM cascading drought pattern.
Central Asia is typically characterized by significant warming in the past years than the average worldwide (Mirzabaev, 2013).
Under significantly warming conditions, annual evapotranspiration (ET) significantly increased during low precipitation and
sequentially amplified the runoff deficit in the alpine (Mastrotheodoros et al., 2020). Zhao et al. (2022) found that previous
studies overestimate the reduction in evaporation from bare soil during droughts in arid climates under water-limited regimes.
410 They found that ET increases during almost half of the drought months worldwide (drought was defined by the deficits in
precipitation and total water storage) as a result of increased atmospheric water demand outweighing the limiting effect of soil
moisture supply on ET. Possible reasons may be that traditional modelling of the ET response to soil moisture stress downplays
the deep soil moisture supply to ET, could better constrain plant drought response traits and ignores the effects of soil structure
on soil hydraulic conductivity.

415 The driving mechanism of large-scale drought evolution is highly complex involving modulators (atmospheric oscillations),
climate drivers (precipitation and temperature), feedback of land surface phenology, and anthropogenic activities. All these
factors and their interactions construct the initial condition and running situation for drought evolution and trigger the variation
of cascading drought patterns. In this study, the diversity of topography and land surfaces complicates the regional climate
regimes of Central Asia. The introduction of spatiotemporal movement in the definition of cascading drought events has
420 resulted in that a cascading drought event may be involved in multiple climatology-land-cover regimes, further adding to the
complexity of identifying the driving mechanism. Therefore, the simple comparison or common correlation method with single
factors, often applied at gauge/catchment scale, may not be appropriate for exploring the driving mechanism of the large-scale
cascading phenomenon. More information and an appropriate attribution framework need to be explored in the next stage.

425

4.2 New framework to detect high-dimensional drought cascades

430 Many studies are customed to link meteorological drought to hydrological drought by point-to-point time series correlation based on the drought index (Geyaert et al., 2018; Guo et al., 2020; Van Loon et al., 2012). These studies identified their lag, attenuation, prolongation, and pooling based on the time series between two drought types. However, these studies are often conducted at a fixed spatial scale, such as at a gauge station or in a catchment, and the spatial variation in drought progression is not considered.

435 More recently, researchers have begun to define three-dimensional single drought events by introducing continuous spatial-temporal motion and, based on this, have adopted temporal and spatial overlap thresholds to determine whether there is a relationship between two drought events (Jiang et al., 2023; Liu et al., 2019a). The method proposed in this study not only introduces spatiotemporal motion, but also integrates the time series correlation method. The daily time scale used in this study provides more detailed time series of drought area changes and more accurate spatial trajectories (Fig.7). The high-resolution

440 time series at daily time scale provides more input data for analysing temporal and spatial movement correlations (Fig.6). Based on the above, the method can detect the relationship without temporal overlap (Table 2 and Fig.6), identify the linkage among more than two types of droughts, and address their temporal orders. It is more suitable to the actual situation of droughts cascade in the real world as the drought evolving along the water circle may span a long period and interrelated droughts do not necessarily present overlap in time. The similarity rule of the space-time motion could break the lots of temporal scale and

445 space pre-restrictions in the conventional methodology and reduce the spatiotemporal incomparability, which is helpful to reduce subjective pre-determination in exploring drought cascades and proceed in recognizing drought cascades more flexibly. Moreover, beyond the four types of droughts discussed in this study, the dynamic spatiotemporal movement can be observed within droughts occurring in different systems, such as the socio-economic system, and other related hazards, such as heatwaves. Consequently, the framework presented in this study offers valuable prospects for identifying multidimensional

450 cascading linkages between different types of hazards.

Farahmand et al. (2021) investigated the cascading drought phenomenon involving precipitation, runoff, soil moisture, and streamflow to explore their temporal structure. This study differs from our work in three aspects. 1) This work did not involve identifying the relationship between different drought events, as they directly linked the most significant drought events in a given region to form a cascading event. 2) Moderate and small drought events were also not considered (e.g., flash droughts).

455 3) They do not take into account area variations and spatial motions during drought progression. The framework proposed in this paper based on the dynamic space-time motion at the daily time scale enables us to capture more sub-seasonal droughts at moderate and small spatial scales (Table 2 and Fig.6), such as flash drought. It will provide a better understanding of the evolution of sub-seasonal drought across multiple systems, which is critical to design more scientific adaptation policies in the face of increased flash drought and related compound extreme events under human-induced climate change.

460 Cascading events, in general, refer to the sequential occurrence of different hazards over time. These events can exhibit correlations from shared drivers, causal mechanisms, or simply by chance. However, distinguishing between these cases poses

a challenge due to limited sample sizes and an incomplete understanding of the intricate system comprising myriad influencing factors (Zscheischler et al., 2020). This challenge is also present in this study, given the limited knowledge of external environmental parameters (e.g., temperature, vegetation, and human activities) in the evolution of droughts. In addition, the

465 cascading connection has proceeded in the spatial area of PCP droughts, and information outside the PCP drought area is not discussed in this work. Furthermore, only one ET/Runoff/SM drought event is identified in each, which may lead to an underestimation of the severity of cascading droughts. Consequently, further research is warranted to explore these aspects in future studies.

5 Conclusion

470 In conclusion, we present a novel daily time-scale framework for detecting cascading droughts across multiple systems in the higher dimension with flexible spatiotemporal overlap, which mainly relies on evaluating the similarity of the dynamic spatiotemporal motion of different types of droughts. This method enables us to recognize cascading drought events incorporating moderate and small drought event (e.g., flash drought). The result exhibits that the four-system cascading drought event is the most common emergent pattern throughout Central Asia. Specifically, ET droughts, Runoff droughts, and SM

475 droughts are more likely to emerge consecutively after the PCP drought, implying the high possibility of the systematic drought risk across the atmosphere, hydrosphere, biosphere, and root zone soil layer throughout CA. The systematic and severe drought risk across multiple systems is more likely to occur when prolonged PCP droughts with high severity/intensity and large spatial extent are observed. Additionally, ET droughts are likely to occur after PCP droughts, often earlier than Runoff droughts, and SM droughts commonly occur at last. ET/Runoff/SM droughts exhibit longer duration than PCP droughts, which might be

480 attributed to the poor recovery capacity of the fragile land surface ecosystem of Central Asia. Furthermore, SM droughts at the root zone layer display the slightest severity and smallest area but the most prolonged duration, suggesting that the fluctuations in drought signal become smoother and broader when they proceed from the atmosphere through depth to the root zone soil. Overall, this work manifests more details of spatial-temporal variations within the drought cascades across multiple systems. In the real world, apart from the four droughts mentioned in this study, droughts in other systems and other related hazards,

485 such as heat waves, involve dynamic space-time motion as well. Therefore, the framework proposed here offers a new possibility to detect dynamic droughts cascade between multiple sequential hazards. The adoption of this framework has the potential to facilitate a comprehensive understanding of the intricate dynamics associated with cascading droughts in various elements of the water cycle. Moreover, its practical significance lies in its ability to effectively assess and predict across-system cascading risks in the context of global warming.

Data availability

Daily precipitation data were obtained from the APHRODITE dataset (http://aphrodite.st.hirosaki-u.ac.jp/download/), which has a spatial resolution of 0.25°×0.25° and covers the period of 1951-2015. The potential and actual ET derived from the GLEAM v3.5a project (https://www.gleam.eu/) at a spatial resolution of 0.25°×0.25° and the daily time scale, covering the period of 1980-2020. Root soil moisture data were obtained from the simulated result of the Noah model GLDAS, which is at a spatial resolution of 0.25°×0.25°, 3-hourly temporal resolution and covered the period from 1948 to 2015 (https://disc.gsfc.nasa.gov/datasets/GLDAS_NOAH025_3H_2.0/summary?keywords=GLDAS_NOAH025_3H_2.0). The daily runoff at the spatial resolution 0.5°×0.5° was from the ISIMIP2a project (https://www.isimip.org/protocol/2a/), covering the period of 1971-2010. The software used to generate all the results is MATLAB 2021b. The code of violin plot was from Bechtold, Bastian, 2016. Violin Plots for Matlab, Github Project https://github.com/bastibe/Violinplot-Matlab, DOI: 10.5281/zenodo.4559847.

Author contribution

LT: conceptualization, methodology, software, formal analysis, investigation, writing- original draft preparation, writing-reviewing and editing, visualization. MD: resources, writing-reviewing, supervision. JH: data curation, formal analysis, writing-reviewing and editing, funding acquisition, supervision, project administration.

Acknowledgements

We acknowledge the financial support from the WE-ACT project funded by the European Commission's Horizon Programme (Grant agreement ID: 101083481). L.T. sincerely thanks Dr. Qing Lin for his support in the writing and coding part of this study. L.T. would like to thank the financial support from the CSC Fellowship.

Competing interests

The authors declare that they have no conflict of interest.

References

AghaKouchak, A.: A baseline probabilistic drought forecasting framework using standardized soil moisture index: application to the 2012 United States drought, Hydrology and Earth System Sciences, 18, 2485-2492, 2014.

Andreadis, K. M., Clark, E. A., Wood, A. W., Hamlet, A. F., and Lettenmaier, D. P.: Twentieth-century drought in the conterminous United States, J. Hydrometeorol., 6, 985-1001, 2005.

Apurv, T., Sivapalan, M., and Cai, X. M.: Understanding the Role of Climate Characteristics in Drought Propagation, Water Resour. Res., 53, 9304-9329, 2017.

Bachmair, S., Kohn, I., and Stahl, K.: Exploring the link between drought indicators and impacts, Nat. Hazards Earth Syst. Sci., 15, 1381-1397, 2015.

520 Barella-Ortiz, A. and Quintana-Segui, P.: Evaluation of drought representation and propagation in regional climate model simulations across Spain, Hydrol. Earth Syst. Sci., 23, 5111-5131, 2019.

Barker, L. J., Hannaford, J., Chiverton, A., and Svensson, C.: From meteorological to hydrological drought using standardised indicators, Hydrol. Earth Syst. Sci., 20, 2483-2505, 2016.

Basara, J. B., Christian, J. I., Wakefield, R. A., Otkin, J. A., Hunt, E. H., and Brown, D. P.: The evolution, propagation, and spread of flash
525 drought in the Central United States during 2012, Environ. Res. Lett., 14, 084025, 2019.

Beck, H. E., Zimmermann, N. E., McVicar, T. R., Vergopolan, N., Berg, A., and Wood, E. F.: Present and future Köppen-Geiger climate classification maps at 1-km resolution, Scientific data, 5, 1-12, 2018.

Christian, J. I., Basara, J. B., Hunt, E. D., Otkin, J. A., Furtado, J. C., Mishra, V., Xiao, X. M., and Randall, R. M.: Global distribution, trends, and drivers of flash drought occurrence, Nat Commun, 12, 11, 2021.

530 Cook, B. I., Mankin, J. S., and Anchukaitis, K. J.: Climate change and drought: From past to future, Current Climate Change Reports, 4, 164-179, 2018.

de Brito, M. M.: Compound and cascading drought impacts do not happen by chance: A proposal to quantify their relationships, Sci. Total Environ., 778, 146236, 2021.

Ding, Y. B., Xu, J. T., Wang, X. W., Cai, H. J., Zhou, Z. Q., Sun, Y. N., and Shi, H. Y.: Propagation of meteorological to hydrological
535 drought for different climate regions in China, J. Environ. Manage., 283, 12, 2021.

Farahmand, A. and AghaKouchak, A.: A generalized framework for deriving nonparametric standardized drought indicators, Adv. Water Resour., 76, 140-145, 2015.

Farahmand, A., Reager, J. T., and Madani, N.: Drought Cascade in the Terrestrial Water Cycle: Evidence From Remote Sensing, Geophys. Res. Lett., 48, 10, 2021.

540 Fouillet, A., Rey, G., Laurent, F., Pavillon, G., Bellec, S., Guihenneuc-Jouyaux, C., Clavel, J., Jougla, E., and Hémon, D.: Excess mortality related to the August 2003 heat wave in France, International archives of occupational and environmental health, 80, 16-24, 2006.

Gaupp, F., Hall, J., Hochrainer-Stigler, S., and Dadson, S.: Changing risks of simultaneous global breadbasket failure, Nature Climate Change, 10, 54-57, 2020.

Geyaert, A. I., Veldkamp, T. I. E., and Ward, P. J.: The effect of climate type on timescales of drought propagation in an ensemble of global
545 hydrological models, Hydrol. Earth Syst. Sci., 22, 4649-4665, 2018.

Ghiggi, G., Humphrey, V., Seneviratne, S. I., and Gudmundsson, L.: GRUN: an observation-based global gridded runoff dataset from 1902 to 2014, Earth Syst. Sci. Data, 11, 1655-1674, 2019.

Guo, H., Bao, A. M., Liu, T., Ndayisaba, F., Jiang, L. L., Zheng, G. X., Chen, T., and De Maeyer, P.: Determining variable weights for an Optimal Scaled Drought Condition Index (OSDCI): Evaluation in Central Asia, Remote Sensing of Environment, 231, 17, 2019.

550 Guo, H., Bao, A. M., Ndayisaba, F., Liu, T., Kurban, A., and De Maeyer, P.: Systematical Evaluation of Satellite Precipitation Estimates Over Central Asia Using an Improved Error-Component Procedure, Journal of Geophysical Research-Atmospheres, 122, 10906-10927, 2017.

Guo, H., Chen, S., Bao, A. M., Hu, J. J., Gebregiorgis, A. S., Xue, X. W., and Zhang, X. H.: Inter-Comparison of High-Resolution Satellite Precipitation Products over Central Asia, Remote Sens., 7, 7181-7211, 2015.

555 Guo, Y., Huang, S. Z., Huang, Q., Leng, G. Y., Fang, W., Wang, L., and Wang, H.: Propagation thresholds of meteorological drought for triggering hydrological drought at various levels, Sci. Total Environ., 712, 12, 2020.

Hsu, H. and Dirmeyer, P. A.: Soil moisture-evaporation coupling shifts into new gears under increasing CO2, Nat Commun, 14, 2023.

Hu, Z. Y., Chen, X., Chen, D. L., Li, J. F., Wang, S., Zhou, Q. M., Yin, G., and Guo, M. Y.: "Dry gets drier, wet gets wetter": A case study over the arid regions of central Asia, Int. J. Climatol., 39, 1072-1091, 2019.

560 Iqbal, M. F. and Athar, H.: Validation of satellite based precipitation over diverse topography of Pakistan, Atmos. Res., 201, 247-260, 2018.

Jamandre, C. A. and Narisma, G. T.: Spatio-temporal validation of satellite-based rainfall estimates in the Philippines, Atmos. Res., 122, 599-608, 2013.

Jiang, L., Jiapaer, G., Bao, A., Kurban, A., Guo, H., Zheng, G., and De Maeyer, P.: Monitoring the long-term desertification process and assessing the relative roles of its drivers in Central Asia, Ecological Indicators, 104, 195-208, 2019.

565 Jiang, S. H., Wei, L. Y., Ren, L. L., Xu, C. Y., Zhong, F., Wang, M. H., Zhang, L. Q., Yuan, F., and Liu, Y.: Utility of integrated IMERG precipitation and GLEAM potential evapotranspiration products for drought monitoring over mainland China, Atmos. Res., 247, 15, 2021.

Jiang, T., Su, X., Zhang, G., Zhang, T., and Wu, H.: Estimating propagation probability from meteorological to ecological droughts using a hybrid machine learning copula method, Hydrol. Earth Syst. Sci., 27, 559-576, 2023.

Jones, E. and van Vliet, M. T. H.: Drought impacts on river salinity in the southern US: Implications for water scarcity, Sci. Total Environ.,
570 644, 844-853, 2018.

Klein, I., Gessner, U., and Kuenzer, C.: Regional land cover mapping and change detection in Central Asia using MODIS time-series, Applied Geography, 35, 219-234, 2012.

Kurc, S. A. and Small, E. E.: Soil moisture variations and ecosystem-scale fluxes of water and carbon in semiarid grassland and shrubland, Water Resour. Res., 43, 2007.

575 Lehner, F., Coats, S., Stocker, T. F., Pendergrass, A. G., Sanderson, B. M., Raible, C. C., and Smerdon, J. E.: Projected drought risk in 1.5 C and 2 C warmer climates, Geophys. Res. Lett., 44, 7419-7428, 2017.

Liu, Y., Zhu, Y., Ren, L., Singh, V. P., Yong, B., Jiang, S., Yuan, F., and Yang, X.: Understanding the spatiotemporal links between meteorological and hydrological droughts from a three-dimensional perspective, Journal of Geophysical Research: Atmospheres, 124, 3090-3109, 2019a.

580 Liu, Y. W., Liu, Y. B., and Wang, W.: Inter-comparison of satellite-retrieved and Global Land Data Assimilation System-simulated soil moisture datasets for global drought analysis, Remote Sensing of Environment, 220, 1-18, 2019b.

Ma, H., Zeng, J., Chen, N., Zhang, X., Cosh, M. H., and Wang, W.: Satellite surface soil moisture from SMAP, SMOS, AMSR2 and ESA CCI: A comprehensive assessment using global ground-based observations, Remote Sensing of Environment, 231, 111215, 2019.

Martens, B., Miralles, D. G., Lievens, H., van der Schalie, R., de Jeu, R. A. M., Fernández-Prieto, D., Beck, H. E., Dorigo, W. A., and

585 Verhoest, N. E. C.: GLEAM v3: satellite-based land evaporation and root-zone soil moisture, Geosci. Model Dev., 10, 1903-1925, 2017.

Mastrotheodoros, T., Pappas, C., Molnar, P., Burlando, P., Manoli, G., Parajka, J., Rigon, R., Szeles, B., Bottazzi, M., Hadjidoukas, P., and Fatichi, S.: More green and less blue water in the Alps during warmer summers, Nature Climate Change, 10, 155-+, 2020.

McKee, T. B. D., Nolan J.; McKee, John Kleist: The relationship of drought frequency and duration to time scales, Eighth Conference on Applied Climatology, 17, 1993.

590 Miralles, D. G., De Jeu, R. A. M., Gash, J. H., Holmes, T. R. H., and Dolman, A. J.: Magnitude and variability of land evaporation and its components at the global scale, Hydrol. Earth Syst. Sci., 15, 967-981, 2011a.

Miralles, D. G., Holmes, T., De Jeu, R., Gash, J., Meesters, A., and Dolman, A.: Global land-surface evaporation estimated from satellite-based observations, Hydrol. Earth Syst. Sci., 15, 453-469, 2011b.

Mirzabaev, A.: Climate Volatility and Change in Central Asia: Economic Impacts and Adaptation, 2013. 2013.

595 Orth, R. and Destouni, G.: Drought reduces blue-water fluxes more strongly than green-water fluxes in Europe, Nat Commun, 9, 2018.

Patrick, E.: Drought characteristics and management in Central Asia and Turkey, FAO Water Reports; Food and Agriculture Organization of the United Nations Rome: Rome, Italy, 2017. 2017.

Pendergrass, A. G., Meehl, G. A., Pulwarty, R., Hobbins, M., Hoell, A., AghaKouchak, A., Bonfils, C. J., Gallant, A. J., Hoerling, M., and Hoffmann, D.: Flash droughts present a new challenge for subseasonal-to-seasonal prediction, Nature Climate Change, 10, 191-199, 2020.

600 Peng, C.-K., Buldyrev, S. V., Havlin, S., Simons, M., Stanley, H. E., and Goldberger, A. L.: Mosaic organization of DNA nucleotides, Physical review e, 49, 1685, 1994.

Peng, C. K., Buldyrev, S. V., Goldberger, A. L., Havlin, S., Sciortino, F., Simons, M., and Stanley, H. E.: Long-range correlations in nucleotide sequences, Nature, 356, 168-170, 1992.

Peng, J., Dadson, S., Hirpa, F., Dyer, E., Lees, T., Miralles, D. G., Vicente-Serrano, S. M., and Funk, C.: A pan-African high-resolution

605 drought index dataset, Earth Syst. Sci. Data, 12, 753-769, 2020.

Podobnik, B. and Stanley, H. E.: Detrended cross-correlation analysis: a new method for analyzing two nonstationary time series, Physical review letters, 100, 084102, 2008.

Sheffield, J., Goteti, G., and Wood, E. F.: Development of a 50-year high-resolution global dataset of meteorological forcings for land surface modeling, Journal of climate, 19, 3088-3111, 2006.

610 Shukla, S. and Wood, A. W.: Use of a standardized runoff index for characterizing hydrologic drought, Geophysical Research Letters, 35, 2008.

Spinoni, J., Barbosa, P., De Jager, A., McCormick, N., Naumann, G., Vogt, J. V., Magni, D., Masante, D., and Mazzeschi, M.: A new global database of meteorological drought events from 1951 to 2016, J. Hydrol.-Reg. Stud., 22, 24, 2019.

Stagge, J. H., Tallaksen, L. M., Gudmundsson, L., Van Loon, A. F., and Stahl, K.: Candidate distributions for climatological drought indices

615 (SPI and SPEI), International Journal of Climatology, 35, 4027-4040, 2015.

Sutanto, S. J., Vitolo, C., Di Napoli, C., D'Andrea, M., and Van Lanen, H. A. J.: Heatwaves, droughts, and fires: Exploring compound and cascading dry hazards at the pan-European scale, Environ. Int., 134, 10, 2020.

Tuttle, S. E. and Salvucci, G. D.: Confounding factors in determining causal soil moisture-precipitation feedback, Water Resour. Res., 53, 5531-5544, 2017.

620 Van Loon, A. F.: Hydrological drought explained, Wiley Interdisciplinary Reviews: Water, 2, 359-392, 2015.

Van Loon, A. F., Van Huijgevoort, M. H. J., and Van Lanen, H. A. J.: Evaluation of drought propagation in an ensemble mean of large-scale hydrological models, Hydrol. Earth Syst. Sci., 16, 4057-4078, 2012.

Vicente-Serrano, S. M., Gouveia, C., Camarero, J. J., Beguería, S., Trigo, R., López-Moreno, J. I., Azorín-Molina, C., Pasho, E., Lorenzo-Lacruz, J., and Revuelto, J.: Response of vegetation to drought time-scales across global land biomes, Proceedings of the National Academy

625 of Sciences, 110, 52-57, 2013.

Vicente-Serrano, S. M., Miralles, D. G., Domínguez-Castro, F., Azorin-Molina, C., El Kenawy, A., McVicar, T. R., Tomás-Burguera, M., Beguería, S., Maneta, M., and Peña-Gallardo, M.: Global Assessment of the Standardized Evapotranspiration Deficit Index (SEDI) for Drought Analysis and Monitoring, Journal of Climate, 31, 5371-5393, 2018.

Xu, K., Yang, D., Xu, X., and Lei, H.: Copula based drought frequency analysis considering the spatio-temporal variability in Southwest China, J. Hydrol., 527, 630-640, 2015.

Yatagai, A., Kamiguchi, K., Arakawa, O., Hamada, A., Yasutomi, N., and Kitoh, A.: APHRODITE: Constructing a long-term daily gridded precipitation dataset for Asia based on a dense network of rain gauges, Bulletin of the American Meteorological Society, 93, 1401-1415, 2012.

Yoo, J., Kim, J., Kwon, H. H., and Kim, T. W.: A new drought monitoring approach using three-dimensional drought properties based on a dynamic drought detection technique algorithm, J. Hydrol.-Reg. Stud., 44, 14, 2022.

Yuan, X., Wang, Y., Ji, P., Wu, P., Sheffield, J., and Otkin, J. A.: A global transition to flash droughts under climate change, Science, 380, 187-191, 2023.

Yusa, A., Berry, P., Cheng, J. J., Ogden, N., Bonsal, B., Stewart, R., and Waldick, R.: Climate change, drought and human health in Canada, Int. J. Environ. Res. Public Health, 12, 8359-8412, 2015.

Zargar, A., Sadiq, R., Naser, B., and Khan, F. I.: A review of drought indices, Environmental Reviews, 19, 333-349, 2011.

Zebende, G. F.: DCCA cross-correlation coefficient: Quantifying level of cross-correlation, Physica A: Statistical Mechanics and its Applications, 390, 614-618, 2011.

Zhao, M., Liu, Y., and Konings, A. G.: Evapotranspiration frequently increases during droughts, Nature Climate Change, 12, 1024-1030, 2022.

Zscheischler, J., Martius, O., Westra, S., Bevacqua, E., Raymond, C., Horton, R. M., van den Hurk, B., AghaKouchak, A., Jezequel, A., Mahecha, M. D., Maraun, D., Ramos, A. M., Ridder, N. N., Thiery, W., and Vignotto, E.: A typology of compound weather and climate events, Nat. Rev. Earth Environ., 1, 333-347, 2020.